JOURNAL OF CATALYSIS 117, 91–101 (1989)

Elementary Steps in the Formation of Highly Dispersed Palladium in NaY

I. Pd Ion Coordination and Migration

S. T. HOMEYER AND W. M. H. SACHTLER[1]

Ipatieff Laboratory, Department of Chemistry, Northwestern University, Evanston, Illinois 60208

Received May 31, 1988; revised November 29, 1988

TPR, TPD, TPO, and TPMS have been used to determine the location and chemical state of Pd supported on NaY. Oxidation of the ammine ligands of $Pd(NH_3)_4^{2+}$ is found to be a stepwise process, producing $Pd(NH_3)_2^{2+}$ ions in supercages and $Pd(NH_3)^{2+}$ and Pd^{2+} ions in sodalite cages. The relative abundance and location of these ions can be controlled by the calcination program. The size of Pd particles after reduction depends on the location and coordination of Pd ions after calcination. Calcination below 250°C leaves Pd ions in the supercages, where their coordination to ammine ligands decreases with increasing calcination temperature. The H/Pd ratio after reduction shows a strong positive correlation with the calcination temperature. It is concluded that the Pd particle size in the kinetic regime is controlled by the relative rates of nucleation and crystal growth, which in this case are determined by the relative abundances of the Pd tetraammine and diammine ions. At a calcination temperature of 300°C Pd ions lose the third ammine ligand allowing the monoammine Pd ions to migrate into sodalite cages, where the remaining ligand is destroyed at 400°C.

INTRODUCTION

The unique properties of zeolites, high ion exchange capability and a crystalline structure with uniform pore diameters, allow preparation of highly dispersed metals with narrow particle size distributions (*1*). Since the pioneering work by Rabo *et al.* (*2*), noble metals on zeolites have been established as important industrial catalysts and considerable research has focused on these systems (*3*). The objective of combining the catalytic properties of transition metals with the steric constraints imposed by zeolite geometries provides strong incentive for research on active and highly selective zeolite-supported transition metal catalysts (*4*).

The location, size, and shape of metal clusters in zeolites are controlled by the method of preparation. The most common method consists of three main steps: ion exchange, calcination, and reduction. Pd or Pt ions are commonly introduced into zeolites by exchange of their tetraammine salts. Ammine removal in N_2 or under vacuum causes autoreduction and migration, resulting in large-particle formation (*5*), but calcination in an oxygen flow can yield high Pt dispersion (*6–8*). Calcination and reduction can be carried out at constant or variable temperatures, permitting a large variety of catalyst preparation programs. The dependence of the ultimate metal dispersion on the calcination temperature is intriguing. An optimum calcination temperature can be defined for obtaining maximum dispersion of Pt in NaY (*6, 9–11*). Metal dispersion is low if calcination is carried out above or below the optimal temperature. In order to better understand these phenomena, research in this laboratory is aimed toward clarifying the elementary processes that occur during calcination and reduction of metal/zeolite systems. Previously we reported on the Pt/NaY (*10–12*), Pt/NaHY

[1] To whom all correspondence should be addressed.

0021-9517/89 $3.00

(*11*), PtCu/NaY (*13*), and Ni/NaY (*14*) systems; the present report deals with Pd/NaY. As an introduction into the problematics on which this paper is focused, the reader is reminded of some well-documented facts and physical laws which are relevant in this context:

(i) In faujasite-type zeolites with moderate Al/Si ratios, there exists a strong thermodynamic driving force for multivalent transition metal ions, which have been stripped of their ligands, to migrate from the supercages to the smallest cages commensurate with their size. The high negative charge density in the sodalite cages or hexagonal prisms is the main cause of this difference in potential energy. The charge density depends, however, on the Al/Si ratio of the zeolite, as Dumesic has quantitatively shown by Monte Carlo calculations (*15*). XRD data by Gallezot *et al.* (*16, 17*) of metal faujasite systems of high metal load confirm unequivocally that migration of bare Pt or Pd ions from the supercages to the sodalite cages is complete after calcination at 500°C for several hours.

(ii) Reduction of metal ions in sodalite cages or hexagonal prisms requires a higher temperature than reduction of the same metal ions in the supercages. Formation of metal–metal bonds, i.e., metal cluster formation, significantly contributes to the thermodynamic driving force for reduction. It follows that under reducing conditions there is a tendency for metal atoms in small cages to leave these sites and migrate to larger cages or the external surface. The direction of this atom migration under reducing conditions is opposite to the direction of ion migration during calcination.

(iii) It follows from elementary principles of physical chemistry that the size of any solid particle formed under dynamic conditions is governed by the ratio of two rates, viz., nucleation and growth (*18–21*). If the growth rate is large compared to the rate of nucleation, the first nuclei will grow into large particles. Conversely, a low growth/nucleation rate ratio results in many small particles. This universal relation must also be valid for the formation of metal particles in supercages during the initial stage, before particle growth becomes limited by cage dimensions. In this initial stage it appears obvious that the growth rate will be limited by transport processes, i.e., the migration of the metal ions to the reduced nuclei. This migration depends on the location of the ions (supercage or sodalite cage) and on their degree of complexation, as the interaction with cage walls will be different for bare metal ions and complexed ions.

There exists, hence, a general consensus on the validity of the physical principles involved and also about the direction of the individual processes: (i) ammine destruction, (ii) ion migration, and (iii) particle formation. However, little is known on the kinetic interplay when these processes occur simultaneously and compete with each other. Under calcination conditions, deammination of the metal ions and ion migration into the smaller cages will often compete. In previous work, it was shown that for Pt/NaY, the processes of deammination of $Pt(NH_3)_4^{2+}$ and migration of Pt^{2+} ions from the supercages to the sodalite cages can be separated; i.e., conditions can be defined where deammination is virtually complete, leaving Pt ions within the supercage network (*11*). This is a rather exceptional situation and unique for Pt. In more general cases these processes will overlap and compete with each other. Under reduction conditions, nucleation and growth processes occur, the latter being controlled by the location and the degree of complexation. Therefore, the preceding processes during catalysts calcination will affect the kinetics of ion reduction and the ultimate metal dispersion. From this we conclude that a detailed study is desirable to unravel the kinetic network of the parallel and consecutive elementary processes involved in the formation of metal particles in zeolites.

The primary goal of this study is to characterize the chemical state and location of Pd in NaY as a function of calcination temperature. This has been accomplished by using TPO (temperature-programmed oxidation), TPR (temperature-programmed reduction), TPD (temperature-programmed desorption), and TPMS (temperature-programmed mass spectrometry) to monitor the rates of O_2 consumption and N_2 production (TPO), H_2 consumption (TPR), H_2 desorption (TPD), and NH_3 desorption (TPMS) by samples calcined to various temperatures. This information leads to a quantitative description of ion migration and relative rates of particles nucleation and growth. The resultant concepts are instrumental for the synthesis of Pd/NaY catalysts with maximum metal dispersion.

METHODS

B1. Sample Preparation

Two different batches (2 and 7 wt%) of Pd supported on NaY were prepared by ion exchange. The exchanges were performed by adding a dilute solution (0.01 *M*) of $[Pd(NH3)_4](NO_3)_2$ (Strem Chemicals, Lot No. 19167) dropwise to a NaY (Linde LZY-52) slurry (1 g/200 ml) at room temperature. The solutions and slurries were prepared using doubly deionized water. Fletcher and Townsend (*22*) have shown that complete exchange is expected with these loadings at room temperature. This was verified via elemental analysis by Galbraith Laboratories.

B2. Calcination Procedure

All samples were calcined under a high flow (180 ml/min) of pure O_2 in a packed bed reactor at atmospheric pressure. The temperature was ramped at 0.5°C from room temperature (RT) to the specified calcination temperature and then held at this temperature for 2 hr. The flow was then switched to Ar (22 ml/min) and the catalyst was cooled to RT in preparation for temperature-programmed studies.

B3. Temperature Programmed Reduction/Desorption

Apparatus. A conventional TPR apparatus (outlined in Fig. 1) was used to determine the TPR and TPD profiles. A molecular sieve cooled to −80°C was positioned before the sample side of the thermal conductivity detector (TCD) to ensure that H_2O and NH_3 did not interfere with H_2 consumption measurements. The TCD was cooled in an ice/water slurry, providing constant response during each run. The analog signals from the thermocouple and TCD were passed through low-noise/high-gain amplifiers and monitored using a high-gain A/D board in a microcomputer. H_2 consumptions, based on area under the curve measurements, were calculated numerically using computer software. The apparatus was calibrated using H_2 injections and crosschecked by the reduction of a known amount of CuO. The error was estimated to be less than 10%.

TPR procedure. Samples consisting of 150 mg of 2 wt% Pd/NaY were used for both TPR and TPD. TPR was performed after calcination to various temperatures. The catalyst was cooled to −80°C in Ar, then the flow was switched to 5% H_2/Ar flow (25 ml/min). The temperature was ramped from −80 to 500°C at 8°C/min.

TPD procedure. The sample was first calcined as stated above, reduced under a 5% H_2/Ar flow (25 ml/min) with a temperature ramp of 8°C/min to 200°C, then held in the H_2/Ar flow at 200°C for 15 min. This constant reduction procedure allows changes in the H/Pd ratio to be considered as a function of calcination temperature only.

A fixed H_2 chemisorption procedure prior to TPD was followed in order to keep the dispersion measurements as consistent as possible. The catalyst was allowed to cool to RT in the H_2/Ar flow and held in this flow for 15 min to ensure complete coverage. Then, the sample was purged in an Ar flow (22 ml/min) at room temperature for 20

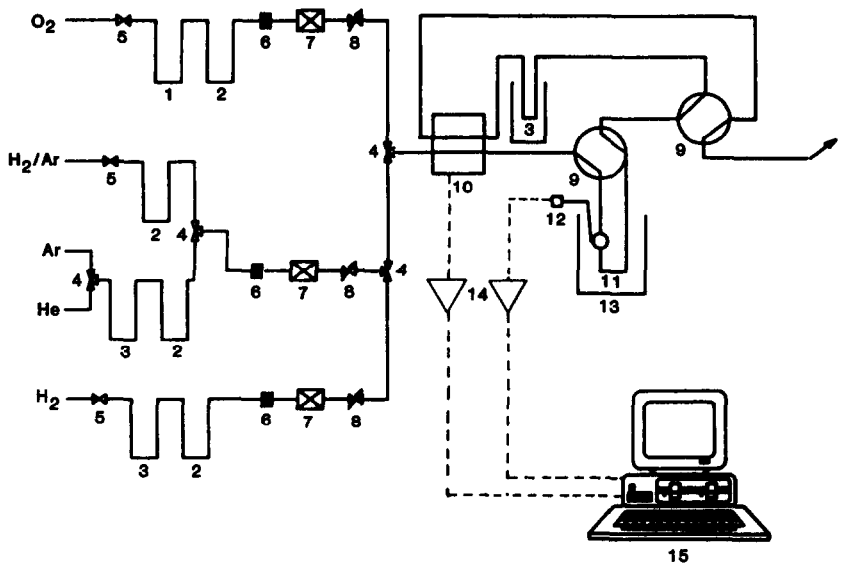

FIG. 1. Diagram of TPR apparatus. Legend: (1) Pt/SiO_2 trap to remove H_2 from O_2. (2) Molecular sieve trap. (3) MnO trap. (4) Three-way valve. (5) On/off valve. (6) Particle filter. (7) Flow meter. (8) Metering valve. (9) Four-way valve. (10) Thermal conductivity detector. (11) Microreactor. (12) Thermocouple. (13) Furnace. (14) Operational amplifiers. (15) Personal computer with A/D board.

min to decompose the Pd hydride (*23*). Finally, the sample was cooled to −80°C in preparation for TPD, which was performed in an Ar flow (22 ml/min) with a temperature ramp of 8°C/min from −80 to 700°C.

TPMS data, discussed in the next section, show that H_2 release at temperatures higher than 350°C is not due to chemisorbed hydrogen; therefore, these late peaks were not included in the dispersion calculations.

TPO procedure. The TPO data were obtained in a flow apparatus similar to that described above. A high-throughput pressure-reducing system combined with a computer-interfaced mass spectrometer (Dycor M200) downstream of the catalyst enabled continuous product analysis of a variety of mass numbers. The TPO was performed on an uncalcined 7 wt% $Pd(NH_3)_4^{2+}$/NaY sample in 5% O_2/He flow (60 ml/min) while the temperature was increased from 23 to 500°C at a heating rate of 8°C/min.

TPMS procedure. Quantitative analysis of desorbed ammonia was performed in a recirculating batch reactor equipped with a Dycor M100 mass spectrometer. A complete description of the apparatus has been provided by Augustine and Sachtler (*24*). Higher metal loading catalysts (7 wt%) were used for TPMS in view of the detection limits of the mass spectrometer. Temperature-programmed desorption of NH_3 was carried out under 38 Torr of H_2. The samples were calcined *in situ* as mentioned above and cooled to RT in an Ar flow (22 ml/min). The temperature was ramped from 23 to 500°C at 8°C/min. The data obtained represent the integral production of mass 15, which is due to fragmentation of NH_3. Numerical differentiation of these data produced NH_3 desorption spectra that could be compared to TPR spectra. Calibration was performed with an uncalcined catalyst and crosschecked with known pressures of pure NH_3 gas.

RESULTS

C1. TPO

The following mass numbers were monitored during TPO of an uncalcined sample:

2 (H_2), 14 (N), 15 (NH), 18 (H_2O), 28 (N_2), 30 (NO), 32 (O_2), and 46 (NO_2). No response was observed for mass numbers 2, 14, 15, 30, and 46. Mass number 18 went off scale in the beginning of the run as expected due to the large H_2O release from the uncalcined zeolite. The consumption of O_2 and the production of N_2 are displayed in Fig. 2.

Quantitative analysis of O_2 consumption is unwise because of a shifting baseline; however, because the rate of N_2 production mirrors the rate of O_2 consumption and the N_2 baseline is stable, quantification can be based on N_2 production. The N_2 spectrum reveals that two of the original four ammine ligands are oxidized with one rate maximum at 270°C. The third ammine ligand is rapidly oxidized, resulting in the sharp peak with a maximum at 340°C. The fourth ammine ligand is burned at higher temperatures (400°C).

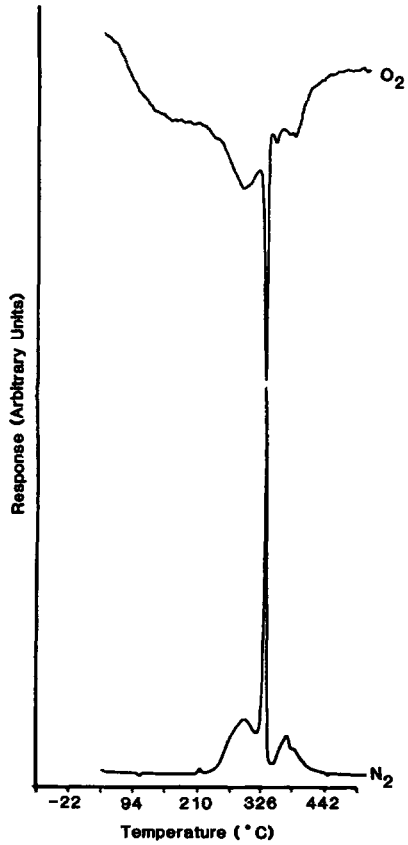

FIG. 2. TPO of 7 wt% $Pd(NH_3)_4^{2+}$/NaY (top profile: O_2 consumption; bottom profile: N_2 production).

Thermogravimetric analysis (TGA) was performed on a hydrated NaY zeolite in an O_2 flow in an effort to determine the water content of the zeolite during calcination. The spectra are not presented here and the data are summarized as follows: at T_C = 100°C, 60% of the physisorbed H_2O is retained by the support, and for $T_C \geq 200$°C, the majority of the water is removed.

C2. TPR/TPMS

Figure 3 gives the TPR spectra (solid lines) with superimposed differentiated TPMS spectra (dotted lines) obtained after calcination to various temperatures. Direct comparison of these spectra can be made after noting that TPR was performed in a flow system and TPMS in a recirculating batch reactor. Table 1 summarizes the quantitative data pertaining to Fig. 3.

The TPR peak profiles can be divided into two groups: peak profiles are sharp in the first group after low-temperature calcination ($T_C \leq 250$°C); broad TPR peaks are characteristic of the second group resulting from high-temperature calcination ($T_C \geq$ 400°C). An intermediate peak profile occurs at T_C = 300°C. In all cases H_2 consumption measurements correspond to complete reduction of Pd^{2+} to Pd^0.

The TPMS data for T_C = 100°C show that there are two main NH_3 desorption peaks: (i) a well-defined peak at low temperatures (180°C) and (ii) a broad peak beginning at 200°C and ending above 500°C. In an attempt to assign these peaks to desorptions of definite species, TPMS of $[Pd(NH_3)_4](NO_3)_2$ and NH_4/Y were performed and their spectra are given in Fig. 4. Comparison of these spectra with that of T_C = 100°C shows that the low-temperature desorption can be attributed to ammonia released during reduction of the metal, and the high-temperature desorption is due to the destruction of ammonium ions created during reduction.

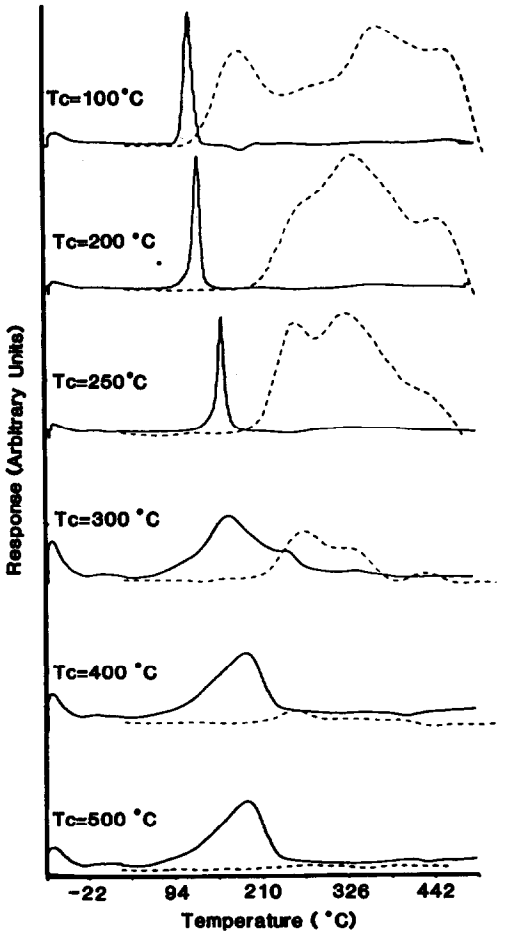

FIG. 3. TPR with superimposed TPMS profiles of 2 wt% $Pd(NH_3)_4^{2+}$/NaY calcined to various temperatures. (Solid lines: H_2 consumption; dotted lines: NH_3 production.)

TABLE 1

TPR/TPMS Data

Calcination temp (°C)	Catalyst color[a]	Reduction rate maxima (°C)	% Pd reduced[b]	% Ammines remaining[a]
100	White	110	102	100
200	Light yellow	120	106	82
250	Yellow	150	108	72
300	Pink	160	97	18
400	Pink	190	97	0
500	Pink	190	99	0

[a] After calcination.
[b] Assuming reduction of Pd^{2+}.

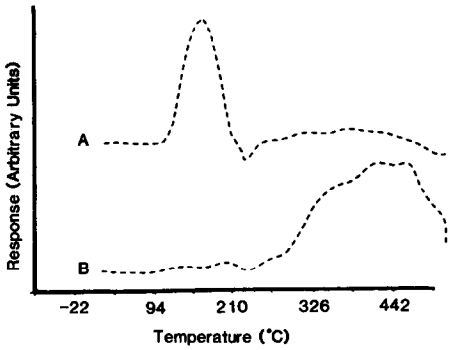

FIG. 4. TPMS of $Pd(NH_3)_4(NO_3)_2$ (profile A) and NH_4^+/NaY (profile B).

TPMS data show that ammine oxidation during calcination begins at T_C = 100°C and is complete by $T_C \geq$ 400°C. This loss of ammine ligands is accompanied by a color change in the sample. The colors of the catalysts after calcination are given in Table 1. Color comparisons with other palladium compounds provide a qualitative indication that ammine coordination decreases and oxygen coordination increases with increasing T_C. $[Pd(NH_3)_4](NO_3)_2$ is white, $Pd(NH_3)_2(OH)_2$ is yellow, and $PdO_2 \cdot xH_2O$ is red.

C3. TPD

Figure 5 shows the TPD spectra obtained after calcination to various temperatures and reduction to 200°C, and Table 2 lists the resultant dispersions. H_2 desorption at high temperatures is a complication in many of the TPD spectra and should be addressed at this point. The late peak in the TPD has been observed for platinum supported on Y zeolite and several explanations have been offered for this behavior (*11*). The decrease in size of this peak with increasing calcination temperature led to the speculation that, in the case of Pd/NaY, the high-temperature peak could be due to ammonia decomposition. In Fig. 6 the percentage ammine left after calcination and the percentage H_2 production at high temperatures are plotted vs calcination temperature. The close correlation of these plots indicates that the H_2

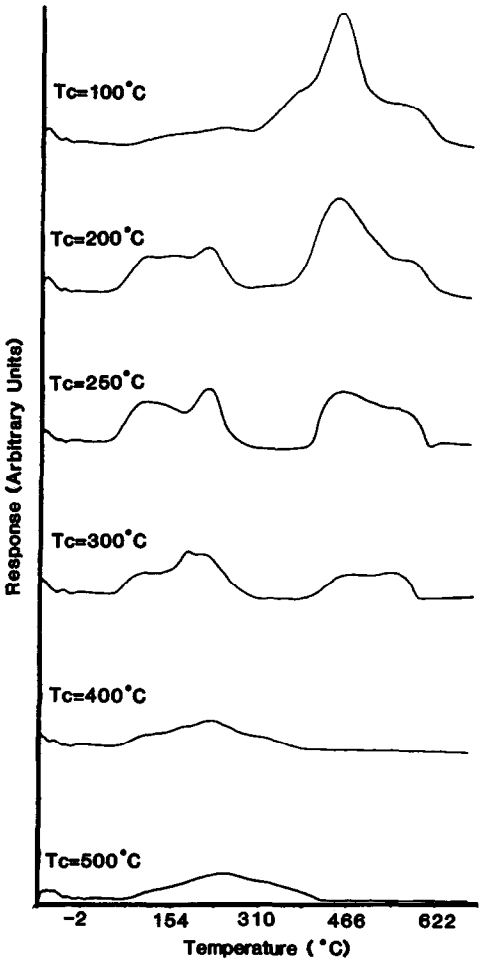

FIG. 5. TPD spectra of 2 wt% Pd/NaY calcined to various temperatures and reduced to 200°C.

TABLE 2

TPD Data

Calcination temp (°C)	Reduction temp (°C)	H/Pd ratio	High-temperature peak (μmol H_2)	Particle size (Å)[a]
100	200	0.28	30	40.0
200	200	0.84	23	13.3
250	200	0.89	13	12.6
300	200	0.67	6	16.7
400	200	0.63	0	17.8
500	200	0.63	0	17.8

[a] Assuming spherical particles.

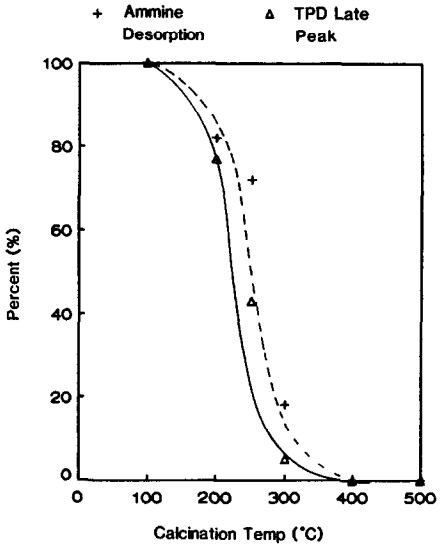

FIG. 6. TPMS/TPD correlation. Percentage ammines left after calcination and percentage H_2 produced at high-temperature TPD vs calcination temperature.

evolved at high temperatures, in an inert environment and in the presence of Pd, could be due to the catalytic decomposition of NH_4^+ formed during reduction. This was confirmed in a separate experiment by monitoring NH_3, H_2, and N_2 evolution during the TPR and TPD (*25*). It was found that under a H_2 flow NH_3 desorption continued above 400°C; however, under an inert flow, NH_3 desorption discontinued at 400°C, and H_2 and N_2 were evolved above 400°C. These data led to the conclusion that H_2 release above 350°C was not due to chemisorption; therefore, it was not included in dispersion measurements.

In separate experiments we confirmed that the increase in the H/Pd ratio truly represents a decrease in average particle size. A trivial possibility, viz., that particles are small, but NH_3 adsorption strongly competes with hydrogen adsorption, could be ruled out: reduction in flowing hydrogen at higher temperatures ($T_R \geq 200$°C) and then cooling the catalyst in H_2 to *RT* does not cause the H/Pd ratio to increase, but decreases it markedly. Another test, based on an observation of Gallezot and Imelik,

makes use of the behavior of Pd/zeolites upon reoxidation (*16*). They found that small Pd particles ($d \leq 20$ Å) become redispersed as Pd^{2+} ions upon oxidation to high temperatures; but larger Pd particles are transformed into PdO. On the basis of this criterion, our TPR data indicate that the particles with low H/Pd are indeed quite large (*25*).

The TPD measurements provide an indication of the location and size of reduced metal particles. Like the TPR spectra, the TPD peak profiles can be divided into two groups, $T_C \leq 250$°C and $T_C \geq 400$°C, with an intermediate profile at $T_C = 300$°C.

For $T_C \leq 250$°C, the desorption profile increases in size and resolution with increasing calcination temperature resulting in a well-defined desorption spectrum at $T_C = 250$°C. The corresponding H/Pd ratios imply a decrease in particle size from 40 Å at $T_C = 100$°C to 13 Å at $T_C = 250$°C. At $T_C = 300$°C, the TPD profile begins to lose resolution and broaden; likewise, the H/Pd ratio (67%) indicates a loss of metal surface. For samples which had been calcined at $T_C \geq 400$°C, desorption occurs with a broad peak profile and the H/Pd ratio remains constant, viz., 63%. A detailed study of the results for $T_C \geq 400$°C will be presented in a following paper.

DISCUSSION

D1. Stepwise Oxidation of Ammine Ligands

Three different reactions that might occur during calcination are:

(i) Release of ammine ligands:

$$Pd(NH_3)^{2+}_{4(zeo)} \rightarrow Pd^{2+}_{(zeo)} + 4NH_{3(g)}$$

(ii) Oxidation of ammine ligands:

$$Pd(NH_3)^{2+}_{4(zeo)} + \tfrac{3}{2}O_{2(g)} \rightarrow Pd^{2+}_{(zeo)} + 2N_{2(g)} + 3H_2O_{(g)}$$

(iii) Autoreduction of Pd by NH_4:

$$Pd(NH_3)^{2+}_{4(zeo)} \rightarrow Pd^0 + 2NH_{3(g)} + N_{2(g)} + 2H_{2(g)} + 2H^+_{(zeo)}$$

The only products observed during TPO are N_2 and H_2O with the production of N_2 mirrored by O_2 consumption. The possibility that autoreduction (reaction (iii)), followed by oxidation of Pd^0 to PdO, takes place can be ruled out on the basis of our TPR data (*25*). These show that PdO, if present, is identified by a TPR peak at 0°C. The lack of any noticeable reduction at 0°C after calcination excludes PdO as a calcination product. H_2 consumptions calculated from TPR data show that, in all cases, Pd is divalent after calcination. Therefore, it can be concluded that calcination in an oxygen flow oxidizes the ammine ligands via reaction (ii), leaving Pd^{2+} coordinated to the zeolite lattice.

The N_2 profile, given in Fig. 2, shows that oxidation of ammine ligands occurs in discrete steps. In the first step two ammine ligands are oxidized. The fact that these are oxidized simultaneously with one rate maximum indicates that $Pd(NH_3)^{2+}_3$ is not a stable calcination product. For low degrees of deammination the population of Pd complexes in the supercages will, therefore, consist of $Pd(NH_3)^{2+}_4$ and $Pd(NH_3)^{2+}_2$. In the second step, the diammine complex decomposes rapidly as evidenced by the extremely sharp spike in Fig. 2. Once $Pd(NH_3)^{2+}$ is formed, higher temperatures are required to oxidize the remaining ligand. The data show that calcination under the conditions outlined in the experimental section can produce four possible products: $Pd(NH_3)^{2+}_4$, $Pd(NH3)^{2+}_2$, $Pd(NH_3)^{2+}$, or Pd^{2+}. The fast step in the oxidation process appears to be the oxidation of the diammine species. The sharp spike characteristic of this step suggests a very strong driving force for the formation of Pd monoammine in the NaY zeolite.

D2. Location and Coordination of Pd^{2+}

A condensed summary of the data obtained from the TPR/TPMS and TPD studies is given in Fig. 7. In it, the ratio of adsorbed hydrogen to palladium (depicted as percentage dispersion), the percentage am-

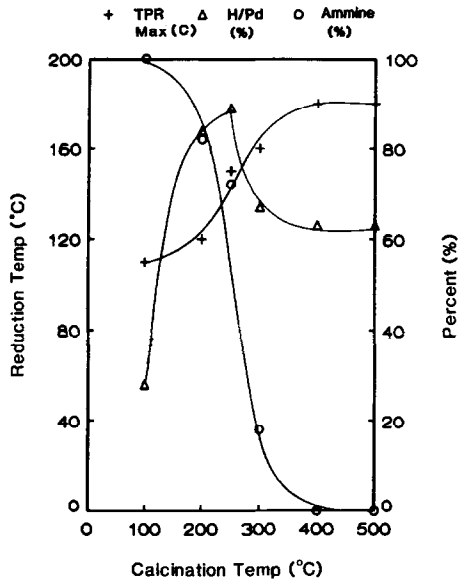

FIG. 7. Percentage ammines remaining after calcination (% ammine), percentage dispersion (% H/Pd), and temperature of reduction rate maxima (TPR max (°C)), vs calcination temperature.

mines remaining after calcination, and the temperature of reduction rate maxima are plotted as a function of calcination temperature. The combined data illustrate several important trends that occur as the the calcination temperature is increased.

The quantitative data of ammine ligand retention, obtained from TPMS, show that oxidation of ammine ligands with the calcination program defined in Section B begins at 100°C and is complete at 400°C, and the curve has an inflection point at 250°C. This inflection point temperature appears highly relevant for the understanding of the kinetics of the processes involved during calcination. Note that the shape of TPR peaks in Fig. 3 also changes abruptly from very sharp to very broad, once the calcination temperature exceeds 250°C. Further, Fig. 7 shows that the temperature where the reduction rate becomes highest depends on the temperature of the previous calcination; and this plot, again, has an inflection point at 250°C. These data, in combination with the changes in color, consistently reveal a rather dramatic change in the situation of the Pd ions when the calcination temperature reaches this critical value. Further evidence for this critical jump is found in the H/Pd values of the reduced catalyst which reflect a rather dramatic effect of the previous calcination program: the H/Pd values increase steeply up to T_C = 250°C; above that value they are markedly lower and remain constant for T_C > 300°C. The combined data show that two separate regimes can be distinguished and that the borderline between the two regimes is between 250 and 300°C.

Combining this new evidence with the facts which were known before and have been summarized in the Introduction, we conclude that up to T_C = 250°C the complexed Pd ions remain in the supercages; above this temperature they move to the sodalite cages. The degree of complexation above and below this transition temperature can be derived from the TPMS data: after ion exchange the Pd ions in the supercages are present as tetraammine Pd ions; during calcination they become partially deamminated. Once the diammine Pd ion loses one of its ligands, the monoammine Pd ion migrates into the sodalite cage. This migration is evidenced by the sharp spike in the TPMS spectrum. Upon calcination to higher temperatures, the last ammine ligand is destroyed.

Adsorbed water is released together with the partial destruction of the ammine ligands in the supercages. TGA results show that at T_C = 100°C, 60% of the physisorbed water is present together with the Pd tetraammine ions in the supercages. At 200°C most of this water has been desorbed and 82% of the ammine ligands are left.

D3. Ion Migration during Reduction

The above data illustrate the importance of ion migration from supercages to sodalite cages during calcination. It is not surprising that reduction of ions in the supercages requires a lower reduction temperature than reduction of isolated or paired ions in the

sodalite cages, and that the resulting Pd particle size will be different. What is less trivial is the remarkable increase in Pd dispersion with calcination temperature within the regime where the Pd ions are inside the supercages. As was indicated in the Introduction, it is expected that the size of the reduced Pd particles will be governed by the ratio of two rates: the rate of nucleation and the rate of growth of the nuclei.

Della Betta and Boudart report that Pt dispersion is low in Pt/NaY if reduction is carried out before deammination is complete (*6*). This observation is very similar to the present one for Pd. These authors speculate that $Pt(NH_3)_2(H)_2$ might be formed. This proposed complex is neutral and can, therefore, coagulate to larger entities. Although we cannot entirely rule out this possibility for palladium, it is difficult to rationalize the steep increase in H/Pd with calcination temperature in terms of this model. We propose a different model which is suggested by the positive correlation of the H/Pd and diammine/tetraammine ratios within the regime where reducible Pd ions are located in supercages. We mentioned above that the tetraammine complex is hydrated for the lowest calcination temperatures. It seems certain that such a fully coordinated complex will have little interaction with the cage walls, whereas the diammine complex will be much more strongly anchored on these walls. It follows that the *mobility* of the tetraammine complex diffusing through supercages will be significantly higher than that of the diammine complex which interacts strongly with the cage walls.

During reduction in flowing hydrogen Pd nuclei will be formed and these will grow to Pd particles. The mechanism of this particle growth requires migration of ions to the nuclei, where they become reduced and incorporated into the growing particles. The resultant dispersion is dominated by the relative rates of nucleation and particle growth and the latter rate is limited by the mobility of the complexed ions. If nucleation is fast and growth is slow, the resulting particles will be small; conversely a high ratio of growth rate to nucleation rate leads to large particles. Upon application of these general principles of particle growth to the situation where $Pd(NH_3)_4^{2+}$ and $Pd(NH_3)_2^{2+}$ coexist in supercages and become reduced by H_2, it appears highly plausible that reduction of the tetraammine complex, having the higher mobility and the lower interaction with the walls, will result in large particles, whereas the diammine complex with more solid anchoring to the cage walls and hence lower mobility appears to be the ideal candidate for the formation of very small Pd particles during reduction. This model, therefore, proposes that the positive correlation of H/Pd and diammine/tetraammine ratios is not coincidental but reflects the general causality between nucleation rate/growth rate and particle size.

CONCLUSIONS

Detailed examination of the processes occurring during calcination of ion-exchanged $Pd(NH_3)_4^{2+}$/NaY shows that the ammine ligands are oxidized to N_2 and H_2O in discrete steps yielding $Pd(NH_3)_4^{2+}$ and $Pd(NH_3)_2^{2+}$ in the supercages. Upon further deammination the $Pd(NH_3)^{2+}$ ion is formed and migrates into sodalite cages. The Pd particle size after reduction is predetermined by location and coordination of the Pd ions after calcination. Results are rationalized in terms of the general principle that the relative rates of nucleation and growth determine the particle size in the kinetic regime. Accordingly, highest dispersion of Pd is achieved by retaining the Pd ions in the supercages and maximizing the diammine/tetraammine ratio.

ACKNOWLEDGMENTS

We gratefully acknowledge support from the U.S. Department of Energy under Contract DE-FG02-87ERA3654. A grant-in-aid by the Engelhard Corporation is also gratefully acknowledged.

REFERENCES

1. Breck, D. W., "Zeolite Molecular Sieves." Wiley, New York, 1974.
2. Rabo, J. A., Pickert, P. E., and Mays, R. L., *Ind. Eng. Chem.* **53,** 733 (1961).
3. Minachev, Kh. M., and Isako, Ya. I., *in* "Zeolite Chemistry and Catalysis" (J. A. Rabo, Ed.), p. 533. American Chemical Society, Washington, DC, 1976.
4. Chow, M., Park, S. H., and Sachtler, W. M. H., *Appl. Catal.* **19,** 349 (1985).
5. Regan, W. J., Chester, A. J., and Kerr, G. T., *J. Catal.* **69,** 89 (1981).
6. Della Betta, R. A., and Boudart, M., "Proceedings, 5th International Congress on Catalysis, Palm Beach, 1972," p. 1329. North-Holland, Amsterdam, 1972.
7. Gallezot, P., Alaran-Diaz, A., Dalmon, J. A., Renouprez, A. J., and Imelik, B., *J. Catal.* **39,** 334 (1975).
8. Tzou, M. S., Jiang, H. J., and Sachtler, W. M. H., *React. Kinet. Catal. Lett.* **35,** 207 (1987).
9. Tzou, M. S., and Sachtler, W. M. H., *in* "Proceedings, 10th North Am. Catal. Soc., San Diego, CA, 1988" (J. W. Ward, Ed.), p. 233.
10. Tzou, M. S., Jiang, H. J., and Sachtler, W. M. H., *Solid State Ionics* **26,** 71 (1988).
11. Tzou, M. S., Teo, B. K., and Sachtler, W. M. H., *J. Catal.* **113,** 220 (1988).
12. Park, S. H., Tzou, M. S., and Sachtler, W. M. H., *Appl. Catal.* **24,** 85 (1986).
13. Moretti, G., and Sachtler, W. M. H., *J. Catal.*, in press.
14. Jiang, H. J., Tzou, M. S., and Sachtler, W. M. H., *Catal. Lett.* **1,** 99 (1988).
15. Aparicio, L. M., Dumesic, J. A., Fang, S. M., Long, M. A., Ulla, M. A., Millman, W. S., and Hall, W. K., *J. Catal.* **104,** 381 (1987).
16. Gallezot, P., and Imelik, B., *Adv. Chem. Ser.* **121,** 66 (1973).
17. Bergeret, G., Gallezot, P., and Imelik, B., *J. Phys. Chem.* **85,** 411 (1981).
18. Volmer, M., and Weber, A., *Z. Phys. Chem.* **119,** 277 (1926).
19. Farkas, A., *Z. Phys. Chem.* **125,** 236 (1927).
20. Zel'dovich, Ya. B., *J. Exp. Theor. Phys.* **12,** 525 (1942).
21. Christiansen, J. A., and Nielsen, A. E., *Z. Elektrochem.* **56,** 465 (1952).
22. Fletcher, P., and Townsend, R. P., *Zeolites* **3,** 129 (1983).
23. Boudart, M., and Hwang, H. S., *J. Catal.* **39,** 44 (1975).
24. Augustine, S. M., and Sachtler, W. M. H., *J. Catal.* **106,** 417 (1987).
25. Homeyer, S., and Sachtler, W. M. H., *J. Catal.*, submitted.